HNPCC mutations in hMSH2 result in reduced hMSH2-hMSH6 molecular switch functions

Christopher D. Heinen,[2] Teresa Wilson,[2,3] Anthony Mazurek, Mark Berardini, Charles Butz, and Richard Fishel[1]

Genetics and Molecular Biology Program, Department of Microbiology and Immunology, Kimmel Cancer Center, Thomas Jefferson University, Philadelphia, Pennsylvania 19107
[1]Correspondence: rfishel@lac.jci.tju.edu
[2]These authors contributed equally to this work.
[3]Present address: Radiation Oncology, University of Maryland, Bressler Research Bldg. 6-013, 655 W. Baltimore St., Baltimore, Maryland 21201.

Summary

Mutations in the human mismatch repair (MMR) gene *hMSH2* have been linked to approximately 40% of hereditary nonpolyposis colorectal cancers (HNPCC). While the consequences of deletion or truncating mutations of *hMSH2* would appear clear, the detailed functional defects associated with missense alterations are unknown. We have examined the effect of seven single amino acid substitutions associated with HNPCC that cover the structural subdomains of the hMSH2 protein. We show that alterations which produced a known cancer-causing phenotype affected the mismatch-dependent molecular switch function of the biologically relevant hMSH2-hMSH6 heterodimer. Our observations demonstrate that amino acid substitutions within hMSH2 that are distant from known functional regions significantly alter biochemical activity and the ability of hMSH2-hMSH6 to form a sliding clamp.

Introduction

The mismatch repair (MMR) machinery has been highly conserved from bacteria to man (for review see Fishel and Wilson, 1997; Kolodner, 1996). While *Escherichia coli* contains a single MutS and MutL, eukaryotes contain multiple MutS homologs (MSH) and MutL homologs (MLH) (Fishel and Wilson, 1997; Kolodner, 1996; Modrich and Lahue, 1996). The mitotic MSH proteins play a fundamental role in DNA mispair recognition while the function of MLH proteins is enigmatic. Five human MSH proteins have been identified that assemble into three functional heterodimers (hMSH2-hMSH3; hMSH2-hMSH6; and hMSH4-hMSH5) (Fishel and Wilson, 1997). The hMSH2-hMSH6 heterodimer recognizes single-nucleotide mismatches and small insertion/deletion loop (IDL) mispairs, while hMSH2-hMSH3 recognizes small and large IDL mispairs. The hMSH4-hMSH5 heterodimer appears to be expressed exclusively during meiosis I/II, and its DNA recognition properties and function are largely unknown (Bocker et al., 1999; Paquis-Flucklinger et al., 1997).

A hallmark of MSH proteins is a highly conserved Walker A/B adenosine nucleotide and magnesium binding domain. Studies of both hMSH2-hMSH6 and hMSH2-hMSH3 have revealed an intrinsic mismatch nucleotide-dependent ATP hydrolysis (ATPase) activity (Berardini et al., 2000; Blackwell et al., 1998; Gradia et al., 1997, 1999, 2000; Mazurek et al., 2002; Wilson et al., 1999). An ATPase cycle can be conceptually divided into two major steps: γ-phosphate hydrolysis and release of the ADP hydrolysis product followed by rebinding of a new ATP (ADP→ATP exchange). The rate-limiting step of the human MSH ATPase has been clearly demonstrated to be mismatch-provoked ADP→ATP exchange (Gradia et al., 1997; Wilson et al., 1999). The exchange of ADP→ATP induces a large conformational transition that results in the formation of a hydrolysis-independent sliding clamp on the DNA (Gradia et al., 1999). The observation that ADP→ATP exchange controls MSH function is similar to well-described G protein molecular switches (Fishel, 1998, 2001). GDP→GTP exchange by G proteins is gated by GDP release, which is often mediated by guanine nucleotide exchange factor(s) (GEF) (Sprang, 1997). The fact that mismatched nucleotides act as a functional homolog of GEFs for the MSH molecular switch further substantiates the analogy to G proteins.

An MMR model that appears most consistent with the available data has been proposed (termed the molecular switch model) (Fishel, 1998, 2001). Other models for MMR have also been proposed that include hydrolysis-dependent translocation (Allen et al., 1997) and static transactivation (Junop et al., 2001). In the molecular switch model, the initiation of MMR is prescribed by the loading of multiple MSH sliding clamps (Gradia

SIGNIFICANCE

Loss of human MMR gene function is the largest contributor to the most frequent cancer predisposition syndrome, HNPCC, and is found in a substantial fraction of sporadic colon, endometrial, ovarian, and upper urinary tract tumors. MMR-deficient tumors progress rapidly through the adenoma-to-carcinoma transition and are resistant to a wide variety of therapeutic agents. Understanding the functional consequences of MMR mutations will help in the development of rapid diagnostic screens and targeted therapeutics.

et al., 1999). While the role of the MLH proteins is unknown, they appear to specifically interact with the MSH proteins (Gu et al., 1998; Habraken et al., 1998). Recruitment of additional machinery is required that ultimately results in the completion of excision repair (Bowers et al., 2000, 2001; Clark et al., 2000; Flores-Rozas et al., 2000). Importantly, the molecular switch functions of hMSH2-hMSH6 and the loading of multiple MSH sliding clamps appear to be a growing feature of competitive models for MMR (Blackwell et al., 1998; Fishel, 1998, 2001; Hsieh, 2001).

The central role of MMR in mutation avoidance has been underlined by its connection to the common cancer susceptibility syndrome hereditary nonpolyposis colorectal cancer (HNPCC) (for review see Muller and Fishel, 2002). HNPCC tumors that originate from defects in MMR genes typically display genome-wide instability (termed microsatellite instability or MSI; for definition see Dietmaier et al., 1997). MSI results from unrepaired replication errors within simple repeat sequences that are normally corrected by the MMR system. The vast majority of HNPCC families have been found to contain an alteration of either *hMSH2* or *hMLH1* (Peltomaki and Vasen, 1997). Mutations of the other MMR genes are either absent (*hMSH3* and *hPMS1*) (Liu et al., 2001) or rare and largely associated with atypical families (*hMSH6*, *hPMS2,* and *hMLH3*) (Kolodner et al., 1999; Wijnen et al., 1999; Wu et al., 2001). These and other studies suggest that the operative heterodimers associated with HNPCC are hMSH2-hMSH6 and hMLH1-hPMS2 (Fishel, 2001).

Single amino acid missense alterations account for approximately 25% of the *hMSH2* mutations found in well-defined HNPCC kindreds (Peltomaki and Vasen, 1997). The functional defects associated with these missense mutations are unknown. We have constructed seven *hMSH2* missense mutations that change amino acids located throughout the structural subdomains identified by extrapolation to the MutS crystal structure (Lamers et al., 2000; Obmolova et al., 2000). In all but one case, the tumors from patients carrying these mutations have been confirmed to display MSI, indicating a general defect in MMR (Borresen et al., 1995; Froggatt et al., 1996; Mary et al., 1994; Moslein et al., 1996; Orth et al., 1994). We have placed these missense mutations into the context of hMSH2-hMSH6, purified the resulting heterodimer, and examined their effect on MSH function using six different biochemical measures. We find that the six missense mutations of hMSH2 that result in MSI cause multiple subtle defects in mispair binding and ATP processing that appear to be magnified into an altered ability to efficiently form sliding clamps. These results suggest that these missense mutations promote tumorigenesis by reducing the molecular switch function(s) of hMSH2-hMSH6 and the number of sliding clamps on mismatched DNA. Evaluation of the remaining missense alteration suggests that it is either a noncontributory polymorphism or affects other functions of hMSH2-hMSH6.

Results

HNPCC missense mutations affect mispair DNA binding

Seven *hMSH2* missense mutations were identified in well-defined HNPCC families (Figure 1). PCR mutagenesis was used to create these seven mutant forms of *hMSH2* and included hMSH2(D167H), hMSH2(K393M), hMSH2(R524P), hMSH2(N596Δ), hMSH2(P622L), hMSH2(G674S), and hMSH2(T905R). The seven missense mutations occur in all the structural subdomains identified in the MutS crystal structure except domain I (Figure 1; Lamers et al., 2000; Obmolova et al., 2000). The hMSH2 mutant proteins were coexpressed in a baculovirus system along with wild-type hMSH6. The heterodimers were purified utilizing an N-terminal His tag fused to the hMSH6 protein that has been previously shown to result in a fully active hMSH2-hMSH6 heterodimer (Gradia et al., 1997). All of the missense mutant forms of hMSH2 were successfully copurified with hMSH6 in an apparent 1:1 ratio (data not shown), indicating that none of these mutations affected the ability of hMSH2 and hMSH6 to interact. This observation confirms previous studies that identified two interaction domains between hMSH2 and hMSH6 but found no effect of missense mutations on the protein-protein interaction (Guerrette et al., 1998).

To determine the effect of these missense mutations on the ability of the hMSH2-hMSH6 heterodimer to recognize and bind DNA mismatches, gel shift analysis was performed with a 41 bp oligonucleotide containing a central G/T mismatch (Gradia et al., 1997). Compared to the wild-type protein, the hMSH2(P622L)-hMSH6 and hMSH2(R524P)-hMSH6 proteins failed to elicit a specific gel shift of the labeled G/T mispair (Figure 2A). These results suggest that the hMSH2(P622L)-hMSH6 and hMSH2(R524P)-hMSH6 proteins confer a fundamental defect in mismatch recognition.

Additionally, we examined mispair binding by total internal reflectance (TIR) using an IAsys biosensor (Affinity Sensors, Cambridge, England) (Figure 2B). TIR measures the real-time accumulation of mass on the surface of a cuvette that is maintained in microscopic equilibrium via continuous stirring of a closed system. The 41 bp oligonucleotide containing a central G/T mispair was attached to the binding surface via a biotin-streptavidin linkage (Mazurek et al., 2002). To calculate the equilibrium dissociation constant ($K_{D(G/T)}$), multiple protein concentrations of hMSH2-hMSH6 wild-type or missense mutant heterodimer were examined and the corresponding real-time binding isotherms calculated. An example of the hierarchy of mispair binding by TIR at a single isotherm is shown (Figure 2B). Interestingly, none of the hMSH2-hMSH6 missense mutant proteins retain the maximum binding (B_{max}) of the wild-type protein. Moreover, between a 2- and 8-fold reduction in $K_{D(G/T)}$ was observed (Table 1). Consistent with the gel shift studies, hMSH2(P622L)-hMSH6 and hMSH2(R524P)-hMSH6 displayed among the highest $K_{D(G/T)}$ (Table 1). The sensitivity of the IAsys system is underlined by the hMSH2(N596Δ)-hMSH6 protein, which appears to behave similarly to the hMSH2(R524P)-hMSH6 protein by TIR (see $K_{D(G/T)}$ data in Table 1) but forms a relatively stable, though less efficient, gel shift.

Steady-state ATP hydrolysis is altered by HNPCC missense mutations

hMSH2-hMSH6 contains an intrinsic ATPase activity that is stimulated by mismatched nucleotides (Gradia et al., 1997). The steady-state ATPase activity of each of the missense mutants was determined by classic Michaelis-Menton analysis. We used the Norit method for examining ATPase activity, which measures the release of inorganic phosphate (Gradia et al., 1997). Previous work has shown the Norit method to be superior to thin-layer chromatography (TLC) or polyacrylamide gel electrophoretic (PAGE) analysis because of the ease of data acquisition, reduced expense, and the large number of analyses that could

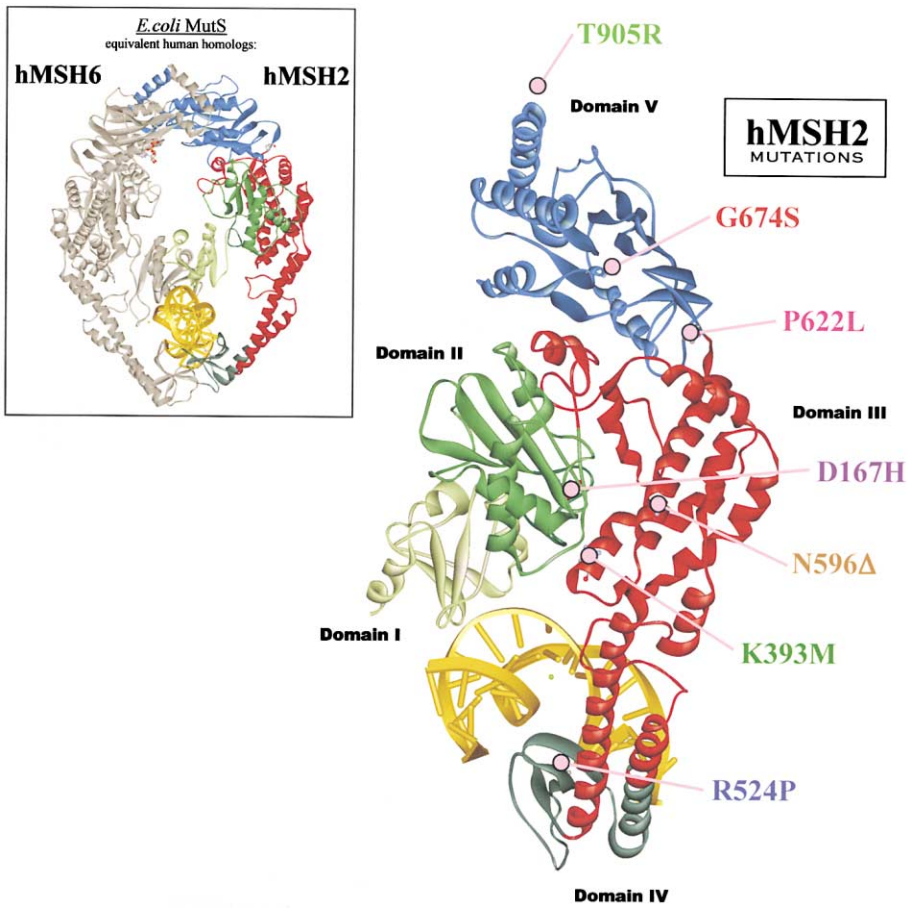

Figure 1. Extrapolated structural location of hMSH2 missense mutations

Insert shows a projection of the hMSH2 and hMSH6 heterodimer subunits onto the *E. coli* MutS homodimer structure (Lamers et al., 2000). The location of amino acids was determined by sequence alignment of hMSH2 with *E. coli* MutS. Subdomains are identified and color-coded. The mispair-containing DNA is shown in yellow. The subunit enlargement has been rotated 30°. The location of the missense mutations examined in this study are marked with pink lines and dots to color-coordinated labels. The hMSH2(T905R) residue is located within a C-terminal region that was removed prior to crystallization.

be performed in tandem. Results of all three methods appear identical (unpublished data).

A substantial deficiency in ATPase activity was observed for both hMSH2(R524P)-hMSH6 and hMSH2(P622L)-hMSH6 (Figure 3A; Table 1). We found that the most reliable assessment of the specific activity of the ATPase associated with a MSH protein preparation was to calculate the catalytic efficiency (K_{cat}/K_M) (Mazurek et al., 2002). There appears to be a general correlation between the catalytic efficiency of the mismatch-dependent ATPase and the $K_{D(G/T)}$ for DNA binding to a G/T mispair (see Figures 2B and 3A and Table 1). This correlation is not surprising since mispair recognition initiates the ATPase cycle (Gradia et al., 1997). Except for the hMSH2(T905R)-hMSH6 protein, all the MSH missense mutant proteins appear to display a significantly reduced catalytic efficiency compared to the wild-type protein. However, none of these missense mutant proteins are completely deficient in ATPase activity. In most cases the catalytic efficiency was reduced to a level that was comparable to the background activity observed with the wild-type protein in the presence of *homoduplex* DNA ($\sim 22 \times 10^4\ M^{-1}\cdot min^{-1}$) (Berardini et al., 2000; Gradia et al., 1997, 1999, 2000; Mazurek et al., 2002; Wilson et al., 1999). Background ATPase activity in the presence of homoduplex DNA appears to be largely the result of nonspecific interaction with DNA ends, a condition that is unlikely to occur in vivo (Gradia et al., 1999).

ATP binding is affected by HNPCC missense mutations

The steady-state ATPase activity of MSH proteins can be further separated into several detectable partial reactions. In addition to mispair recognition, the ATPase cycle requires release of bound ADP followed by ATP binding (ADP→ATP exchange), the formation of a sliding clamp, hydrolysis-independent diffusion/dissociation of this sliding clamp from the end of the oligonucleotide substrate, and finally, recycling of the MSH protein to its initial mispair recognition form by γ-phosphate hydrolysis (Gradia et al., 1999).

We examined ATP binding activity using filter retention of labeled ATP (Figure 3B) and UV crosslinking of labeled ATP (Figure 3C) by the MSH heterodimer proteins. These and other methods of measuring ATP binding activity were found to produce similar results. Because of the relative simplicity of processing large numbers of samples and the likelihood that the nucleotide remains in the triphosphate form throughout the analysis, binding to the poorly hydrolyzable analog of ATP, ATPγS, was measured ($K_{D(ATP)}$) (Figure 3B; Table 1). Previous studies suggested that ATP binding was largely unaffected by the addition of exogenous homoduplex or heteroduplex DNA (Gradia et al., 2000). However, to maintain the distinction between ATP binding and mispair recognition efficiencies, we examined the binding affinity of hMSH2-hMSH6 missense mutant proteins for ATPγS in the absence of added DNA.

We found that all of the hMSH2-hMSH6 missense mutant

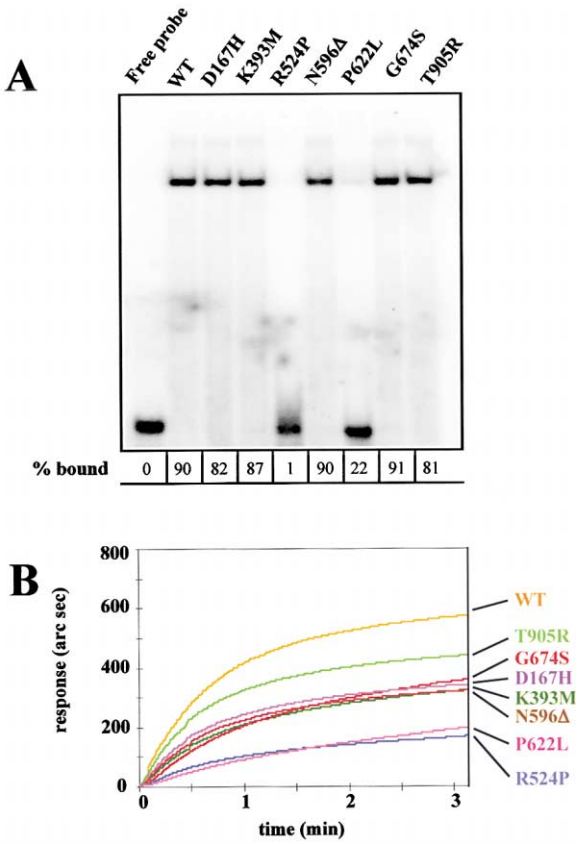

Figure 2. Mispair binding activity of HNPCC missense mutations

A: Gel mobility shift assay of wild-type hMSH2/hMSH6 and HNPCC mutants. The proteins were incubated with a mismatch (G/T) in the presence of 25 μM ADP at 37°C for 5 min followed by electrophoreses in a 5% polyacrylamide gel for 2.5 hr at 4°C. **B:** IAsys Biosensor TIR analysis of hMSH2/hMSH6 and HNPCC mutants. An overlay of the association curves determined with 50 nM concentration of each protein with a G/T mismatch is displayed. Multiple TIR binding experiments using variable concentrations of each hMSH2/hMSH6 protein were performed to determine association (K_A) and dissociation (K_D) constants. From these values, an equilibrium dissociation constant ($K_{D(G/T)}$) was calculated for the interaction of each protein with a G/T mismatch (see Table 1).

proteins displayed a modestly reduced affinity for adenosine nucleotide compared to the wild-type protein (Figure 3B; Table 1). The hMSH2(P622L)-hMSH6 protein appeared substantially deficient for ATPγS binding (Figure 3B; Table 1). These results are consistent with a fundamental defect of this heterodimer protein to process adenosine nucleotide. As a general rule, the affinity for ATPγS appeared to recapitulate the steady-state ATPase activity of the mutant proteins (Table 1; Figures 3A and 3B). The exception was the hMSH2(R524P)-hMSH6 protein, which efficiently bound ATPγS, yet appears defective for its steady-state ATPase. These latter results suggest that ATP binding and mispair-dependent hydrolysis are dissociated within the hMSH2(R524P)-hMSH6 protein.

The hMSH2-hMSH6 heterodimer contains two ATP binding protomers. The efficiency of ATP binding by the individual subunits was examined by UV crosslinking of labeled ATPγS to the hMSH2-hMSH6 heterodimer (Figure 3C). We found that ATPγS binding by the hMSH2 subunit appeared compromised in many of the missense mutations compared to the wild-type protein (Figure 3C). Taken as a whole, the ATPγS crosslinking studies largely recapitulate the ATPγS filter binding results (compare Figure 3B with Figure 3C and Table 1). However, these crosslinking studies appear to be the first to directly examine binding by individual subunits as a mechanism for MSH heterodimer dysfunction. A disconnect between the binding affinity of individual subunits was observed for the hMSH2(R524P), hMSH2(P622L), hMSH2(G674S), and hMSH2(T905R) proteins. We found that ATPγS binding by the hMSH2(G674S) subunit was reduced, a likely result of its location within the Walker A (P loop) region (domain V; Figure 1) involved in contacting the γ-phosphate of ATP. The hMSH2(P622L)-hMSH6 protein results in a hMSH2 peptide that appears completely deficient in ATPγS binding while its heterodimeric partner hMSH6 retains a substantial binding activity. Finally, the hMSH2(R524P) subunit displayed reduced ATP binding activity, yet appeared to enhance ATP binding by the hMSH6 subunit. These results suggest that both independent and interactive functions between the subunits of the hMSH2-hMSH6 heterodimer may be uniquely affected by the missense mutations.

ADP→ATP exchange is affected by HNPCC missense mutations

We examined mismatch-provoked ADP→ATP exchange by the hMSH2-hMSH6 missense mutant heterodimer (Figure 4A). To

Table 1. Kinetic constants of wild-type and mutant hMSH2-hMSH6 protein binding to G/T mismatch DNA, ATPase efficiency in the presence of a G/T mismatch, ATPγS binding, and protein dissociation from a G/T mismatch in the presence or absence of ATP as determined by total internal reflection

	DNA Binding			ATPase		ATPγS Binding	Sliding Clamp Dissociation	
	k_{assoc} 10^{-4} sec^{-1} nM^{-1}	k_{dissoc} 10^{-3} sec^{-1}	$K_{D(G/T)}$ nM	K_M μM	$K_{cat}/K_M \times 10^{4*}$ $M^{-1}min^{-1}$	$K_{D(ATP)}$ μM	$k_{off(buffer\ only)}$ 10^{-3} sec^{-1}	$k_{off(ATP)}$ 10^{-3} sec^{-1}
hMSH2-hMSH6 (WT)	4.0 ± 0.3	6.1 ± 0.9	15.3	43.3	42.3	1.0	2.0 ± 0.1	329.0 ± 30.3
hMSH2(D167H)-hMSH6	1.8 ± 0.6	10.9 ± 2.0	60.5	27.6	27.5	1.8	2.2 ± 0.2	389.0 ± 22.5
hMSH2(K393M)-hMSH6	1.6 ± 0.3	7.0 ± 1.0	43.8	46.3	22.2	2.4	2.1 ± 0.1	186.0 ± 24.9
hMSH2(R524P)-hMSH6	1.5 ± 0.3	10.8 ± 2.0	72.1	158.5	1.9	1.6	27.0 ± 6.4	42.3 ± 2.6
hMSH2(N596Δ)-hMSH6	1.3 ± 0.5	11.4 ± 1.5	88.0	46.7	16.1	2.9	2.1 ± 0.2	314.0 ± 32.9
hMSH2(P622L)-hMSH6	0.7 ± 0.1	6.8 ± 0.6	97.1	**	**	186.0	5.3 ± 0.3	5.0 ± 0.1
hMSH2(G674S)-hMSH6	2.3 ± 0.3	8.3 ± 1.0	36.1	26.3	22.4	1.6	2.0 ± 0.2	305.0 ± 13.1
hMSH2(T905R)-hMSH6	2.8 ± 0.3	7.2 ± 0.9	25.7	29.4	38.1	1.5	1.8 ± 0.1	311.0 ± 17.2

*For comparison, the K_{cat}/K_M for hMSH2-hMSH6 in the presence of a homoduplex oligonucleotide is 22.0 × 10^4 M^{-1}·min^{-1} (Mazurek et al., 2002).
**Insufficient ATPase activity to accurately determine.

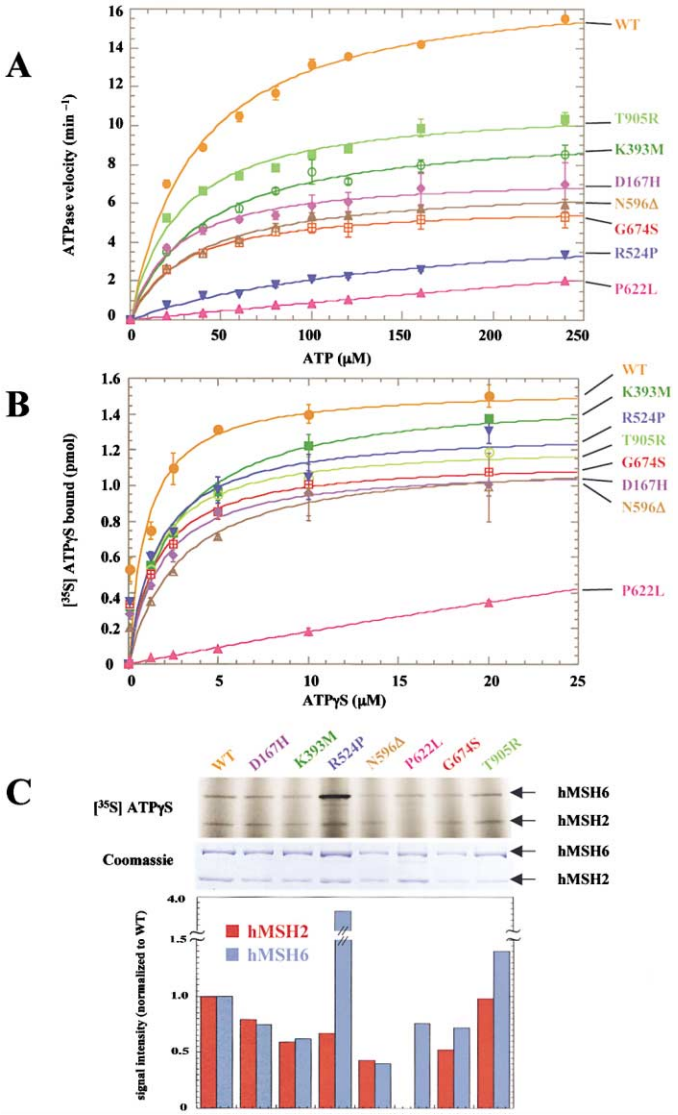

Figure 3. Steady-state ATPase and ATP binding activity of missense mutations

A: Steady-state ATPase. ATPase assays were performed with multiple concentrations of each protein (to ensure <20% total hydrolysis) except for hMSH2(R524P) and hMSH2(P622L) where 150 nM protein was used as a result of their low ATPase activity. The assays contained 240 nM G/T heteroduplex DNA, 17 nM [γ-^{32}P]ATP, and increasing concentrations of unlabeled ATP as shown on the x axis. Following incubation at 37°C for 30 min, the amount of released [γ-^{32}P] was determined (Gradia et al., 1997). **B:** ATP binding activity. 100 nM of each protein was incubated with the indicated concentrations of ATPγS. The reactions were incubated at 37°C for 15 min, and the amounts of ATPγS bound were determined by filter binding. **C:** [^{35}S]ATPγS binding to individual hMSH2 or hMSH6 subunits. Phosphorimaging of Coomassie-stained gel, the Coomassie-stained gel showing the position of the hMSH2 and hMSH6 proteins, and quantitation of [^{35}S] signal from the phosphorimager are shown. Binding and analysis are detailed in the Experimental Procedures.

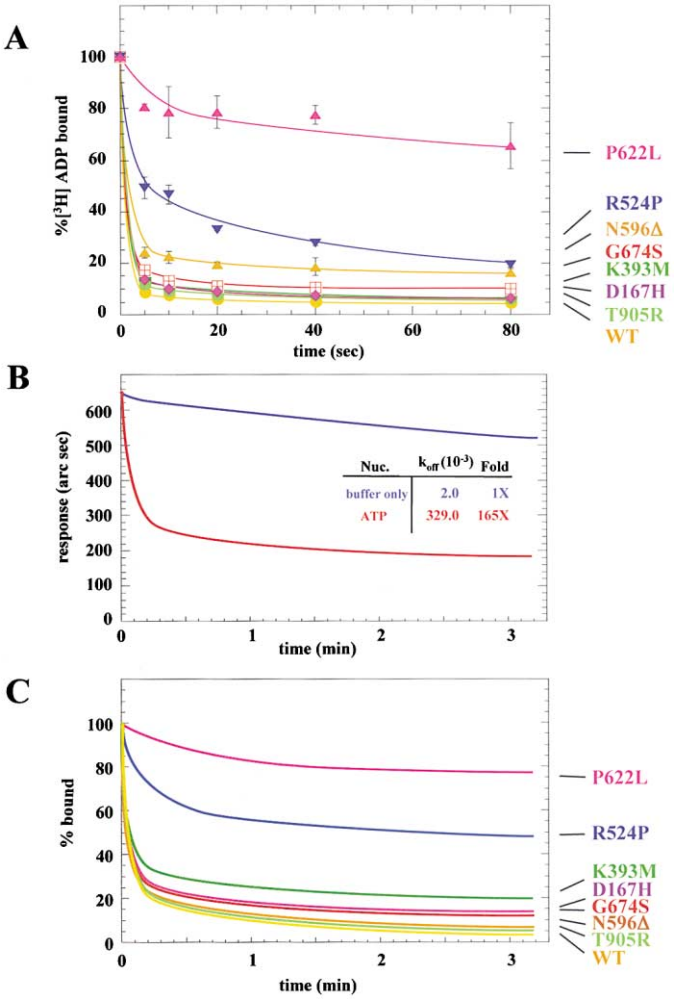

Figure 4. ADP→ATP exchange activity

A: Adenosine nucleotide exchange was performed by preincubating 40 nM of each protein with [^{3}H]ADP followed by the addition of excess unlabeled ATP. After incubation at 37°C for the specified time, the remaining [^{3}H]ADP bound to the protein complexes was determined by filter binding. **B and C:** TIR analysis of hMSH2-hMSH6 dissociation from a mismatched oligonucleotide. **B:** We washed 50 nM of wild-type hMSH2-hMSH6 bound to a G/T mismatch in the IAsys biosensor with buffer alone or buffer containing 250 μM ATP. The corresponding off-rate (K_{off}) values are displayed. **C:** TIR studies of the dissociation from a mismatched oligonucleotide. The dissociation curves for each protein in the presence of 250 μM ATP are displayed as a function of percentage of protein initially bound to the mismatch. From these curves and the corresponding buffer-only dissociation curves (not shown), K_{off} values were calculated.

perform ADP→ATP exchange studies, purified proteins were initially bound with radiolabeled ADP, and then at time zero, excess unlabeled ATP was added to start the reaction (Gradia et al., 1997). Approximately 80% of the bound ADP was released within 5 s for the wild-type and most of the hMSH2-hMSH6 missense mutant proteins. These correspond to a half-rate of mismatch-provoked ADP→ATP exchange $t_{1/2}$ = 0.2–2 s. The exceptions were the hMSH2(R524P)-hMSH6 and hMSH2(P622L)-hMSH6, where the $t_{1/2}$ was ~10 sec and ~180 sec, respectively. The hMSH2(P622L)-hMSH6 protein was found to bind approximately 20% of the initial radiolabeled ADP compared to the wild-type protein, a result consistent with the ATPγS binding studies (see Figures 3B and 3C). ADP→ATP exchange revealed that the hMSH2(P622L)-hMSH6 protein never released more than ~20% of the initially bound ADP over the time course of the experiment (Figure 4A). These results suggest that the hMSH2(P622L)-hMSH6 protein possesses multiple defects in mispair binding and ATP processing. In contrast, the

hMSH2(R524P)-hMSH6 protein bound near wild-type levels of ADP (see Figure 3B). Yet it took ~80 s to release 80% of the bound ADP during ADP→ATP exchange. This observation suggests that the ability of a mispair to provoke ADP→ATP exchange by the hMSH2(R524P)-hMSH6 protein is likely to be one of its major functional defects. The hMSH2(N596Δ)-hMSH6 protein displayed a modest deficiency in mismatch-provoked ADP→ATP exchange ($t_{1/2} \approx 4$ s), which appears consistent with its elevated $K_{D(G/T)}$ values for mispair binding (Figure 2B; Table 1). Taken together, these results support the idea that mispair recognition and ADP→ATP exchange are linked to MSH function and that defects in this dynamic process are associated with HNPCC.

HNPCC missense mutations affect ATP-dependent dissociation from a mismatch

The exchange of ADP→ATP results in the release of hMSH2-hMSH6 from a mispaired oligonucleotide in the form of a sliding clamp (Blackwell et al., 1998; Gradia et al., 1997, 1999). Using TIR, the rate of hMSH2-hMSH6 protein dissociation from the 41 bp oligonucleotide containing a central G/T mismatch was measured following addition of the binding buffer alone ($k_{off(buffer)} = 2.0 \pm 0.1$ ms^{-1}) (Figure 4B). The addition of ATP to the dissociation buffer increased the rate of hMSH2-hMSH6 protein release approximately 165-fold ($k_{off(ATP)} = 329.0 \pm 30.3$ ms^{-1}) (Figure 4B). Because the hMSH2-hMSH6 missense mutant proteins were found to bind the G/T mismatch substrate to differing extents (see Figure 2B), a visual comparison of release from the mismatch was developed by computing the *relative* ATP-induced dissociation (Figure 4C). The relative ATP-induced dissociation displays the release of each protein after setting the initially bound material to 100% (Figure 4C). The *absolute* ATP-induced dissociation rates for buffer alone ($k_{off(buffer)}$) and in the presence of ATP ($k_{off(ATP)}$) were calculated directly from the primary IAsys TIR dissociation data (Table 1).

We observed both dramatic and modest differences in $k_{off(buffer)}$ and $k_{off(ATP)}$ when the hMSH2-hMSH6 missense mutant proteins were compared to the wild-type protein (Figure 4C; Table 1). However, the differences between the hMSH2(D167H)-hMSH6, hMSH2(N596Δ)-hMSH6, hMSH2(G674S)-hMSH6, and hMSH2(T905R)-hMSH6 missense mutant proteins and the wild-type protein appeared to be within experimental error. In contrast, the hMSH2(P622L)-hMSH6 protein was substantially defective in $k_{off(ATP)}$ (compare $k_{off(buffer)}$ with $k_{off(ATP)}$; Figure 4C). Defects in $k_{off(ATP)}$ were found for the hMSH2(R524P)-hMSH6 protein and to a lessor degree for the hMSH2(K393M)-hMSH6 protein. In addition, the hMSH2(R524P)-hMSH6 protein displayed a significant defect in $k_{off(buffer)}$, a result that is consistent with the k_{dissoc} determined by the TIR binding studies. Taken together with the ADP→ATP exchange results, these observations appear to suggest that the hMSH2(R524P)-hMSH6 protein does not form a stable long-term interaction with mismatched DNA, which then affects its subsequent ATP processing. It is important to note the correlation between ATP-induced dissociation from the 41-mer G/T mismatch and the ADP→ATP exchange activity for the individual hMSH2 missense mutations. This correlation is consistent with the concept that ADP→ATP exchange and not ATP hydrolysis induces the formation of an activated MSH molecule capable of dissociating from a mismatch (Fishel, 1998, 2001; Gradia et al., 1997, 1999).

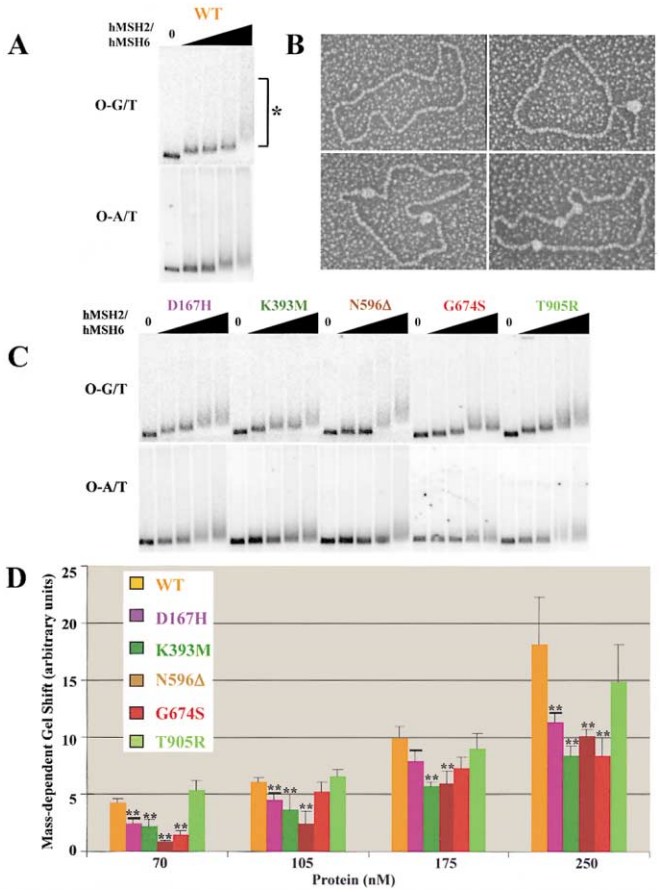

Figure 5. Efficiency of loading multiple sliding clamps onto a circular DNA containing a G/T mismatch

A: Wild-type hMSH2-hMSH6 binding to circular homoduplex DNA (O-A/T) and circular DNA containing a single G/T mismatch (O-G/T). Proteins (70, 105, 175, and 250 nM) were incubated with a ^{32}P-labeled closed circular plasmid DNA containing a single G/T mismatch in the presence of 25 μM ADP at 37°C for 5 min. 250 μM ATP was then added and allowed to incubate an additional 10 min. These reactions were subjected to electrophoresis through a 1% TAE gel, and changes in the mobility of the DNA were measured relative to a DNA-only control. **B:** Electron microscopy of hMSH2-hMSH6 bound to the O-G/T substrate. Representative molecules are shown ranging from unbound to 3 bound hMSH2-hMSH6 proteins per circular substrate. EM quantitation was reported in Gradia et al. (1999). **C:** Binding of hMSH2-hMSH6 missense mutant proteins to the O-G/T substrate. Reactions were performed as described for **A**. The hMSH2(R524P) and hMSH2(P622L) were not tested since they did not produce a stable gel shift. **D:** Quantitative analysis of **A** and **C** relative to the DNA-only control. Arbitrary distance units are shown. Error bars were calculated from the standard error from three independent experiments; statistically significant difference compared to the wild-type protein (p value < 0.05) are marked with double asterisk.

HNPCC mutations reduce the formation of redundant ATP-bound sliding clamps

We examined the loading of multiple sliding clamps onto a 3 kb circular DNA substrate containing a single G/T mismatch (Figure 5). Consistent with previous studies, the addition of wild-type hMSH2-hMSH6 in the presence of ATP (or ATPγS) resulted in a protein concentration-dependent reduction in mobility of these 3 kb DNA substrates (Figure 5A; Gradia et al., 1999). At the highest protein concentration (250 nM), the reduction in mobility extended nearly to the well (see asterisk in Figure 4A). By comparison, at similar high concentrations of wild-type

hMSH2-hMSH6 protein, a modest smearing of the homoduplex control DNA substrate was observed (Figure 4A). Electron microscopic (EM) examination suggested that the reduction in the mobility was due to the loading of multiple hMSH2-hMSH6 sliding clamps into the 3 kb DNA mismatch-containing substrate (Figure 5B). A comprehensive analysis of these EM observations is detailed in Gradia et al. (1999).

With the exception of hMSH2(T905R)-hMSH6, we found that none of the missense mutant proteins consistently shifted the 3 kb circular DNA substrate to an extent similar to the wild-type protein (Figures 4C and 4D). hMSH2(R524P)-hMSH6 and hMSH2(P622L)-hMSH6 are not shown since they were unable to bind to the small mispaired oligonucleotide DNA substrates (Figure 2B). We determined the average reduction in mobility compared to the unshifted control DNA substrate (Figure 4D). These results suggest a consistent and significant reduction in the ability of all the missense mutant proteins, except hMSH2(T905R)-hMSH6, to shift the 3 kb circular substrate containing a mismatch. Together with the mispair binding and adenosine nucleotide activation studies, we conclude that the functional defect associated with bona fide *hMSH2* missense mutations translates to inefficient loading of multiple ATP bound sliding clamps.

Discussion

HNPCC missense mutations affect the coordination of mispair binding with adenosine nucleotide processing

We have examined seven *hMSH2* missense mutations suggested to be causative of HNPCC in well-defined kindreds. While it is likely that distinct missense mutations located within any of the recognized subdomains of the MutS structure may affect the function differently (see Figure 1), we chose these seven mutations to cover the maximum number of structural subdomains. A wide range of specific functional defects were found associated with these *hMSH2* HNPCC missense mutations when placed in the context of the hMSH2-hMSH6 heterodimer. The mispair equilibrium dissociation constant ($K_{D(G/T)}$) for all of the mutant proteins was reduced 2- to 8-fold. A reduced mispair binding was largely reflected in a lowered catalytic efficiency (K_{cat}/K_M) for the hMSH2-hMSH6 ATPase. Remarkably, the catalytic efficiency of the hMSH2(R594P)-hMSH6 and hMSH2(P622L)-hMSH6 proteins was reduced 10- and ~1000-fold, respectively. With the exception of the hMSH2(T905R), the catalytic efficiency of the remaining missense mutations was lowered to the level of wild-type hMSH2-hMSH6 in the presence of homoduplex oligonucleotide DNA (Mazurek et al., 2002). Although the hMSH2(P622L) and hMSH2(R524P) missense mutants fail to form a gel shift, the other five missense mutant proteins appear to form relatively normal gel shifts. These observations suggest that TIR is substantially more effective than gel shift analysis at accurately determining the mispair binding properties of MMR proteins.

Correlating structure with function

Extrapolation of the bacterial MutS structure to the human homologs has suggested that the intrinsic asymmetry between protomers is conserved within the consensus MSH2/MSH6 subunits (Lamers et al., 2000; Obmolova et al., 2000). Biochemical, genetic, and structural comparisons have proposed that the hMSH6 subunit is involved in direct interrogation of the mispair, while the hMSH2 subunit binds the DNA phosphate backbone around the mispair (Biswas and Hsieh, 1997; Bowers et al., 1999; Drotschmann et al., 2001; Dufner et al., 2000; Lamers et al., 2000; Malkov et al., 1997; Obmolova et al., 2000); both protein subunits additionally form half of a clamp structure around the DNA (see Figure 1). The hMSH2(P622L) residue is located at the junction connecting the ATP binding domain (domain V) with a "transmitter" α helix (domain III; see Figure 1). The transmitter α helix terminates in a "clasp region" (domain IV) that appears to capture the mispaired DNA and promote a physical interaction with the mismatch (domain I; see Figure 1). The hMSH2(N596Δ) residue is located within the transmitter α helix (domain III), and the hMSH2(R524P) residue is located within the clasp region (domain IV). The MSH2(D167H) residue is located in domain II, which connects domain I to the body of the hMSH2 (MutS) clamp. These four missense mutations reduce the $K_{D(G/T)}$ for mispair binding 5- to 8-fold (Table 1). In most cases, both the k_{assoc} and k_{dissoc} rates appear to be equally affected (Table 1). However, the hMSH2(P622L) displays a dramatic and unique effect on k_{assoc}, suggesting a near complete defect in the ability to initially interact with the mismatched DNA. The hMSH2(N596Δ)-hMSH6 and hMSH2(R524P)-hMSH6 proteins showed a substantially decreased k_{assoc} and increased k_{dissoc}, suggesting an inability of these transmitter (domain III) and clasp (domain IV) alterations to maintain a stable mispair interaction. Similarly, the hMSH2(D167H)-hMSH6 protein appears to destabilize the mispair recognition process, presumably by affecting the connection of the mispair interaction region (domain I) with the body of the MutS clamp.

Three missense mutations [hMSH2(K393M), hMSH2(G674S), and hMSH2(T905R)] displayed less dramatic effects on the K_D for mispair binding (2- to 3-fold). The close proximity of hMSH2(K393) to several amino acids in domain II opens the possibility that hMSH2(K393M) affects stabilizing interactions between domains II and III (see Figure 1). This alteration appears to have a modest affect on mispair binding but a dramatic affect on ATP-dependent dissociation from the mismatch and the steady-state ATPase. The hMSH2(G674S) missense alteration is located within the highly conserved Walker A (P loop) region and exhibits reduced ATP binding activity by the hMSH2 subunit and background ATPase activity. This result is consistent with reports detailing other P loop mutations and indicates a defect in coordinating ATP processing activity in spite of rather modest mispair binding defects. Finally, the hMSH2(T905R)-hMSH6 protein does not appear to display any consistently significant defects in the biochemical assays used in this study.

Reduced threshold signaling may account for functional defects associated with HNPCC mutants

Signaling networks have been suggested to place a value on a cellular signal such that it is either converted into a biologically relevant event or safely dissipated within the network (Jordan et al., 2000). The sustained amplitude of the signal determines its value. Signaling networks that interface over multiple pathways generally employ a threshold signaling process, which implies that both the amplitude and location are important for biological conversion (Jordan et al., 2000). One aspect of the molecular switch model proposes that the number of MSH sliding clamps specifies a threshold (amplitude and location) for the initiation of MMR (Fishel, 1998, 1999, 2001). The concept of a threshold

signal in MMR appears to be supported by recent real-time observations of GFP-tagged bacterial MutS and MutL (Smith et al., 2001). Smith et al. found MutS and/or MutL proteins associate with chromosomes in a small number of discrete foci that substantially increase in size and location upon induction of DNA damage (Smith et al., 2001). The fluorescent signal of these growing damage-induced foci coalesced at defined locations behind a moving replication fork and must a priori contain large numbers of GFP-tagged molecules to be visible. These studies are most consistent with a threshold signaling process.

The efficient formation of multiple signaling MSH sliding clamps requires a cascade of events that is initiated with mispair recognition and is consummated by appropriate ATP processing with consequent conformational transitions. We found that all of the hMSH2 missense mutations, except hMSH2(T905R), were reduced in their ability to load multiple sliding clamps onto mispair-containing DNA (Figure 5). EM studies found a maximum of 3–5 hMSH2-hMSH6 proteins associated with a 3 kb circular mismatch-containing DNA substrate (Gradia et al., 1999). However, we noted that the glutaraldehyde crosslinking procedure used to prepare samples for EM appeared to strikingly diminish the extent of the mobility reduction observed by gel shift analysis (data not shown). Thus, it is likely that the large reductions in mobility of the 3 kb DNA substrate are the result of substantially more hMSH2-hMSH6 molecules per circular substrate than determined by EM, although the exact number is unknown. Our results demonstrate that defects in one or several of the individual recognition and/or ATP processing catalytic steps culminates in reduced molecular switch function(s) of hMSH2-hMSH6, fewer sliding clamps, and an increased likelihood that a mismatch/lesion signal will be dissipated without biological conversion.

With the exception of hMSH2(T905R), tumors carrying the missense mutations examined here have been shown to display MSI (Borresen et al., 1995; Mary et al., 1994; Moslein et al., 1996; Orth et al., 1994). These observations suggest that the majority of missense mutations examined in this study result in a general defect in MMR. Our results suggested two possibilities: (1) the hMSH2(T905R) missense mutation affects its interaction with downstream machinery effectively disengaging the signal transduction process, or (2) the hMSH2(T905R) alteration is a noncontributory polymorphism. Interestingly, several members of the hMSH2(T905R) family present with numerous adenomatous polyps, a phenotype that is inconsistent with HNPCC (Froggatt et al., 1996). This observation appears to support the notion that the hMSH2(T905R) alteration is either a noncontributory polymorphism or a low-variation. Such possibilities further validate the clinical importance of performing functional studies.

Experimental procedures

Construction of hMSH2 mutations

The hMSH2 mutations were generated utilizing a two-primer PCR mutagenesis protocol (Guerrette et al., 1998). The mutant and wild-type hMSH2-hMSH6 heterodimers were overexpressed and purified from baculovirus as previously described (Gradia et al., 1997). Protein concentrations were determined by measuring the absorbance at 280 nm. In order to control for preparation inconsistencies, we independently purified the hMSH2-hMSH6 missense mutant proteins a minimum of three times. While the data for a single preparation of the purified hMSH2-hMSH6 missense mutant protein is shown, we found independent preparations to produce consistent results (data not shown).

Gel mobility shift assays

DNA oligonucleotides were obtained from Midland Certified Reagent Co. (Midland, TX). We prepared 41 bp DNA heteroduplexes containing a central G/T mismatch (top, 5′-GCT TAG GAT CAT CGA GGA TCG AGC TCG GTG CAA TTC AGC GG-3′; bottom, 5′-CCG CTG AAT TGC ACC GAG CTT GAT CCT CGA TGA TCC TAA GC-3′) as described (Gradia et al., 1997). 25 and 100 nM of each hMSH2-hMSH6 heterodimer was incubated with 9 fmol of ^{32}P-labeled DNA substrate in a buffer containing 100 mM NaCl, 25 mM HEPES-NaOH (pH 8.1), 1 mM EDTA, 25 μM ADP, 15% glycerol, and 20 ng of 200 base pair homoduplex competitor in a final reaction volume of 20 μl. The reactions were incubated at 37°C for 5 min and immediately placed on ice. The samples were electrophoresed on a 5% polyacrylamide (29:1 bis), 4% glycerol gel in TBE buffer. The gels were dried, visualized using a Molecular Dynamics PhosphorImager, and quantified using ImageQuant software. Circular DNA gel shift assays were performed similarly using 3 kb nicked circular heteroduplex DNA substrates generated as described (Gradia et al., 1999). Reactions were incubated with hMSH2-hMSH6 wild-type and mutant proteins at 37°C for 5 min followed by the addition of 250 μM ATP and further incubation at 37°C for 10 min. The circular substrates were electrophoresed on a 1% TAE agarose gel, dried, visualized using a Molecular Dynamics PhosphorImager, and quantified using ImageQuant software.

ATPase assays

ATPase assays were performed with multiple concentrations of each hMSH2-hMSH6 heterodimer (except for hMSH2(R524P) and hMSH2(P622L), which were assayed at 150 nM protein because of their low-level ATPase activity) in 25 mM HEPES-NaOH (pH 8.1), 100 mM NaCl, 10 mM $MgCl_2$, 1 mM dithiothreitol (DTT), and 15% glycerol (Mazurek et al., 2002). The reactions were incubated at 37°C for 30 min, and the fraction of hydrolyzed [γ-^{32}P]ATP was determined by charcoal binding as described previously (Gradia et al., 1997).

ADP→ATP exchange assays

We preincubated 40 nM of each heterodimer for 10 min at 25°C in 25 mM HEPES-NaOH (pH 8.1), 100 mM NaCl, 1 mM DTT, 2 mM $MgCl_2$, 2.3 μM [^{3}H]ADP, and 15% glycerol. Heteroduplex DNA (240 μM) and ATP (25 μM) were added to start the reaction. The reaction was stopped by the addition of 4 ml ice-cold stop buffer (25 mM HEPES-NaOH [pH 8.1], 100 mM NaCl, 10 mM $MgCl_2$) followed immediately by filtering through a Millipore HAWP filter as previously described (Gradia et al., 1997). The filters were subsequently dried, placed into scintillation fluid overnight, and quantitated using a Beckman counter.

ATPγS binding

We incubated 100 nM hMSH2-hMSH6 with varying concentrations of ATPγS (as noted in the figure legend) in 25 mM HEPES-NaOH (pH 8.1), 100 mM NaCl, 10 mM $MgCl_2$, 1 mM DTT, and 15% glycerol. The reactions were incubated at 37°C for 15 min followed by filtration through a Millipore HAWP filter as previously described (Gradia et al., 1997). The filters were subsequently dried, placed into scintillation fluid, and quantitated using a Beckman counter.

ATPγS crosslinking

Binding of [^{35}S]ATPγS to wild-type and mutant proteins was carried out in 10 μl of buffer containing 25 mM HEPES (pH 8.1), 100 mM NaCl, 5 mM $MgCl_2$, 1 mM DTT, 11% glycerol, 150 nM protein, and 0.5 μM [^{35}S]ATPγS (1250 Ci/mmol, 12.5 mCi/ml) and incubated at 37°C for 20 min. The samples were transferred to ice and irradiated for 5 min in a UV Stratalinker 1800 chamber (Stratagene). Samples were then separated on a 7% SDS polyacrylamide gel followed by drying onto Whatman filter paper. Visualization and quantitation was performed using the Molecular Dynamics phosphorimaging system and ImageQuant software. Approximately 0.7 μg of each protein was loaded onto a separate gel and stained with Coomassie blue in order to accurately normalize the relative amount of each mutant protein to that of wild-type. The normalized signal intensity was calculated as follows: $(S_{mutant\ subunit}/S_{wild\text{-}type\ subunit})(C_{wild\text{-}type}/C_{mutant})$, where S is the band intensity from [^{35}S]ATPγS phosphorimaging and C is the sum of the band intensities from both subunits in the Coomassie blue-stained gel.

Total internal reflection analysis

Real-time interaction between hMSH2-hMSH6 proteins and mismatched DNA was performed using the IAsys Biosensor (Affinity Sensors, Cambridge, England). We attached 41 bp duplex oligonucleotides containing a single, central G/T mismatch via a biotin-streptavidin-biotin linkage to an IAsys cuvette. Indicated concentrations of wild-type and mutant hMSH2-hMSH6 were added in the presence of 25 mM HEPES (pH 8.1), 110 mM NaCl, 1 mM DTT, 2 mM $MgCl_2$, 2% glycerol, and 25 μM ADP. The protein was incubated with the mismatched DNA until saturation was reached (generally 3 to 5 min). Association and dissociation constants were determined using FastFit (Affinity Sensors) and GraFit (Erithacus Software) software analyses. For protein dissociation studies, after binding saturation was reached, unbound protein was removed and replaced with a similar buffer containing no protein and either 250 μM ATP or no nucleotide as indicated.

Electron microscopy

EM was performed as previously described (Gradia et al., 1999). Quantitative analysis of these studies is contained in Gradia et al. (1999).

Acknowledgments

The authors wish to thank Jack Griffith (University of North Carolina-Lineberger Cancer Center) for permission to present the electron microscopy panel that was originally part of a previous publication; K. Yoder and S. Acharya for editorial comments and discussion; and C. Schmutte for helpful discussions and the preparation of Figures 1 and 4. This work was supported by National Institutes of Health grants CA67007 and CA72027.

Received: May 9, 2002
Revised: May 29, 2002

References

Allen, D.J., Makhov, A., Grilley, M., Taylor, J., Thresher, R., Modrich, P., and Griffith, J.D. (1997). MutS mediates heteroduplex loop formation by a translocation mechanism. EMBO J. *16*, 4467–4476.

Berardini, M., Mazurek, A., and Fishel, R. (2000). The effect of O^6-methylguanine DNA adducts on the adenosine nucleotide switch functions of hMSH2-hMSH6 and hMSH2-hMSH3. J. Biol. Chem. *275*, 27851–27857.

Biswas, I., and Hsieh, P. (1997). Interaction of MutS protein with the major and minor grooves of a heteroduplex DNA. J. Biol. Chem. *272*, 13355–13364.

Blackwell, L.J., Bjornson, K.P., and Modrich, P. (1998). DNA-dependent activation of the hMutSalpha ATPase. J. Biol. Chem. *273*, 32049–32054.

Bocker, T., Barusevicius, A., Snowden, T., Rasio, D., Guerrette, S., Robbins, D., Schmidt, C., Burczak, J., Croce, C.M., Copeland, T., et al. (1999). hMSH5: a human MutS homologue that forms a novel heterodimer with hMSH4 and is expressed during spermatogenesis. Cancer Res. *59*, 816–822.

Borresen, A.L., Lothe, R.A., Meling, G.I., Lystad, S., Morrison, P., Lipford, J., Kane, M.F., Rognum, T.O., and Kolodner, R.D. (1995). Somatic mutations in the hMSH2 gene in microsatellite unstable colorectal carcinomas. Hum. Mol. Genet. *4*, 2065–2072.

Bowers, J., Sokolsky, T., Quach, T., and Alani, E. (1999). A mutation in the MSH6 subunit of the *Saccharomyces cerevisiae* MSH2-MSH6 complex disrupts mismatch recognition. J. Biol. Chem. *274*, 16115–16125.

Bowers, J., Tran, P.T., Liskay, R.M., and Alani, E. (2000). Analysis of yeast MSH2-MSH6 suggests that the initiation of mismatch repair can be separated into discrete steps. J. Mol. Biol. *302*, 327–338.

Bowers, J., Tran, P.T., Joshi, A., Liskay, R.M., and Alani, E. (2001). MSH-MLH complexes formed at a DNA mismatch are disrupted by the PCNA sliding clamp. J. Mol. Biol. *306*, 957–968.

Clark, A.B., Valle, F., Drotschmann, K., Gary, R.K., and Kunkel, T.A. (2000). Functional interaction of proliferating cell nuclear antigen with MSH2-MSH6 and MSH2-MSH3 complexes. J. Biol. Chem. *275*, 36498–36501.

Dietmaier, W., Wallinger, S., Bocker, T., Kullmann, F., Fishel, R., and Ruschoff, J. (1997). Diagnostic microsatellite instability: definition and correlation with mismatch repair protein expression. Cancer Res. *57*, 4749–4756.

Drotschmann, K., Yang, W., Brownewell, F.E., Kool, E.T., and Kunkel, T.A. (2001). Asymmetric recognition of DNA local distortion. Structure-based functional studies of eukaryotic Msh2-Msh6. J. Biol. Chem. *276*, 46225–46229.

Dufner, P., Marra, G., Raschle, M., and Jiricny, J. (2000). Mismatch recognition and DNA-dependent stimulation of the ATPase activity of hMutSalpha is abolished by a single mutation in the hMSH6 subunit. J. Biol. Chem. *275*, 36550–36555.

Fishel, R. (1998). Mismatch repair, molecular switches, and signal transduction. Genes Dev. *12*, 2096–2101.

Fishel, R. (1999). Signaling mismatch repair in cancer. Nat. Med. *5*, 1239–1241.

Fishel, R. (2001). The selection for mismatch repair defects in hereditary nonpolyposis colorectal cancer: revising the mutator hypothesis. Cancer Res. *61*, 7369–7374.

Fishel, R., and Wilson, T. (1997). MutS homologs in mammalian cells. Curr. Opin. Genet. Dev. *7*, 105–113.

Flores-Rozas, H., Clark, D., and Kolodner, R.D. (2000). Proliferating cell nuclear antigen and Msh2p-Msh6p interact to form an active mispair recognition complex. Nat. Genet. *26*, 375–378.

Froggatt, N.J., Brassett, C., Koch, D.J., Evans, D.G., Hodgson, S.V., Ponder, B.A., and Maher, E.R. (1996). Mutation screening of MSH2 and MLH1 mRNA in hereditary non-polyposis colon cancer syndrome. J. Med. Genet. *33*, 726–730.

Gradia, S., Acharya, S., and Fishel, R. (1997). The human mismatch recognition complex hMSH2-hMSH6 functions as a novel molecular switch. Cell *91*, 995–1005.

Gradia, S., Subramanian, D., Wilson, T., Acharya, S., Makhov, A., Griffith, J., and Fishel, R. (1999). hMSH2-hMSH6 forms a hydrolysis-independent sliding clamp on mismatched DNA. Mol. Cell *3*, 255–261.

Gradia, S., Acharya, S., and Fishel, R. (2000). The role of mismatched nucleotides in activating the hMSH2-hMSH6 molecular switch. J. Biol. Chem. *275*, 3922–3930.

Gu, L., Hong, Y., McCulloch, S., Watanabe, H., and Li, G.M. (1998). ATP-dependent interaction of human mismatch repair proteins and dual role of PCNA in mismatch repair. Nucleic Acids Res. *26*, 1173–1178.

Guerrette, S., Wilson, T., Gradia, S., and Fishel, R. (1998). Interactions of human hMSH2 with hMSH3 and hMSH2 with hMSH6: examination of mutations found in hereditary nonpolyposis colorectal cancer. Mol. Cell. Biol. *18*, 6616–6623.

Habraken, Y., Sung, P., Prakash, L., and Prakash, S. (1998). ATP-dependent assembly of a ternary complex consisting of a DNA mismatch and the yeast MSH2-MSH6 and MLH1-PMS1 protein complexes. J. Biol. Chem. *273*, 9837–9841.

Hsieh, P. (2001). Molecular mechanism of DNA mismatch recognition. DNA Repair *386*, 71–87.

Jordan, J.D., Landau, E.M., and Iyengar, R. (2000). Signaling networks: the origins of cellular multitasking. Cell *103*, 193–200.

Junop, M.S., Obmolova, G., Rausch, K., Hsieh, P., and Yang, W. (2001). Composite active site of an ABC ATPase: MutS uses ATP to verify mismatch recognition and authorize DNA repair. Mol. Cell *7*, 1–12.

Kolodner, R. (1996). Biochemistry and genetics of eukaryotic mismatch repair. Genes Dev. *10*, 1433–1442.

Kolodner, R.D., Tytell, J.D., Schmeits, J.L., Kane, M.F., Das Gupta, R., Weger, J., Wahlberg, S., Fox, E.A., Peel, D., Ziogas, A., et al. (1999). Germ-line msh6 mutations in colorectal cancer families. Cancer Res. *59*, 5068–5074.

Lamers, M.H., Perrakis, A., Enzlin, J.H., Winterwerp, H.H., de Wind, N., and Sixma, T.K. (2000). The crystal structure of DNA mismatch repair protein MutS binding to a G × T mismatch. Nature *407*, 711–717.

Liu, T., Yan, H., Kuismanen, S., Percesepe, A., Bisgaard, M.L., Pedroni, M., Benatti, P., Kinzler, K.W., Vogelstein, B., Ponz de Leon, M., et al. (2001). The role of hPMS1 and hPMS2 in predisposing to colorectal cancer. Cancer Res. *61*, 7798–7802.

Malkov, V.A., Biswas, I., Camerini-Otero, R.D., and Hsieh, P. (1997). Photocross-linking of the NH2-terminal region of Taq MutS protein to the major groove of a heteroduplex DNA. J. Biol. Chem. *272*, 23811–23817.

Mary, J.L., Bishop, T., Kolodner, R., Lipford, J.R., Kane, M., Weber, W., Torhorst, J., Muller, H., Spycher, M., and Scott, R.J. (1994). Mutational analysis of the hMSH2 gene reveals a three base pair deletion in a family predisposed to colorectal cancer development. Hum. Mol. Genet. *3*, 2067–2069.

Mazurek, A., Berardini, M., and Fishel, R. (2002). Activation of human MutS homologs by 8-oxo-guanine DNA damage. J. Biol. Chem. *277*, 8260–8266.

Modrich, P., and Lahue, R. (1996). Mismatch repair in replication fidelity, genetic recombination, and cancer biology. Annu. Rev. Biochem. *65*, 101–133.

Moslein, G., Tester, D.J., Lindor, N.M., Honchel, R., Cunningham, J.M., French, A.J., Halling, K.C., Schwab, M., Goretzki, P., and Thibodeau, S.N. (1996). Microsatellite instability and mutation analysis of hMSH2 and hMLH1 in patients with sporadic, familial and hereditary colorectal cancer. Hum. Mol. Genet. *5*, 1245–1252.

Muller, A., and Fishel, R. (2002). Mismatch repair and the hereditary nonpolyposis colorectal cancer syndrome (HNPCC). Cancer Invest. *20*, 102–109.

Obmolova, G., Ban, C., Hsieh, P., and Yang, W. (2000). Crystal structures of mismatch repair protein MutS and its complex with a substrate DNA. Nature *407*, 703–710.

Orth, K., Hung, J., Gazdar, A., Bowcock, A., Mathis, J., and Sambrook, J. (1994). Genetic instability in human ovarian cancer cell lines. Proc. Natl. Acad. Sci. USA *91*, 9495–9499.

Paquis-Flucklinger, V., Santucci-Darmanin, S., Paul, R., Saunieres, A., Turc-Carel, C., and Desnuelle, C. (1997). Cloning and expression analysis of a meiosis-specific MutS homolog—the human MSH4 gene. Genomics *44*, 188–194.

Peltomaki, P., and Vasen, H.F. (1997). Mutations predisposing to hereditary nonpolyposis colorectal cancer: database and results of a collaborative study. The International Collaborative Group on Hereditary Nonpolyposis Colorectal Cancer. Gastroenterology *113*, 1146–1158.

Smith, B.T., Grossman, A.D., and Walker, G.C. (2001). Visualization of mismatch repair in bacterial cells. Mol. Cell *8*, 1197–1206.

Sprang, S.R. (1997). G protein mechanisms: insights from structural analysis. Annu. Rev. Biochem. *66*, 639–678.

Wijnen, J., de Leeuw, W., Vasen, H., van der Klift, H., Moller, P., Stormorken, A., Meijers-Heijboer, H., Lindhout, D., Menko, F., Vossen, S., et al. (1999). Familial endometrial cancer in female carriers of MSH6 germline mutations. Nat. Genet. *23*, 142–144.

Wilson, T., Guerrette, S., and Fishel, R. (1999). Dissociation of mismatch recognition and ATPase activity by hMSH2-hMSH3. J. Biol. Chem. *274*, 21659–21664.

Wu, Y., Berends, M.J., Sijmons, R.H., Mensink, R.G., Verlind, E., Kooi, K.A., van dDer Sluis, T., Kempinga, C., van der Zee, A.G., Hollema, H., et al. (2001). A role for MLH3 in hereditary nonpolyposis colorectal cancer. Nat. Genet. *29*, 137–138.